European Journal of Pharmaceutics and Biopharmaceutics 190 (2023) 171–183

Contents lists available at ScienceDirect

European Journal of Pharmaceutics and Biopharmaceutics

journal homepage: www.elsevier.com/locate/ejpb

Research paper

Tailoring the release of drugs having different water solubility by hybrid polymer-lipid microparticles with a biphasic structure

Serena Bertoni [a], Beatrice Albertini [a,*], Joanna Ronowicz-Pilarczyk [b], Nadia Passerini [a]

[a] Department of Pharmacy and Biotechnology, Alma Mater Studiorum—University of Bologna, Via S. Donato 19/2, Bologna 40127, Italy
[b] Department of Inorganic and Analytical Chemistry, Faculty of Pharmacy, Collegium Medicum in Bydgoszcz, Nicolaus Copernicus University in Toruń, Jurasza 2, Bydgoszcz 85-089, Poland

ARTICLE INFO

Keywords:
Multicompartment microparticles
PEG/lipid emulsions
Spray congealing
Controlled release
Supersaturation
Oral delivery
Multicores-shell structure
Raman imaging

ABSTRACT

The aim of this study is to investigate the potential of hybrid polymer-lipid microparticles with a biphasic structure (b-MPs) as drug delivery system. Hybrid b-MPs of Compritol®888 ATO as main lipid constituent of the shell and polyethylene glycol 400 as core material were produced by an innovative solvent-free approach based on spray congealing. To assess the suitability of hybrid b-MPs to encapsulate various types of APIs, three model drugs (fluconazole, tolbutamide and nimesulide) with extremely different water solubility were loaded into the polymeric core. The hybrid systems were characterized in terms of particle size, morphology and physical state. Various techniques (e.g. optical, Confocal Raman and Scanning Electron Microscopy) were used to investigate the influence of the drugs on different aspects of the b-MPs, including external and internal morphology, properties at the lipid/polymer interface and drug distribution. Hybrid b-MPs were suitable for the encapsulation of all drugs (encapsulation efficiency > 90 %) regardless the drug hydrophobic/hydrophilic properties. Finally, the drug release behaviors from hybrid b-MPs were studied and compared with traditional solid lipid MPs (consisting of only the lipid carrier). Due to the combination of lipid and polymeric materials, hybrid b-MPs showed a wide array of release profiles that depends on their composition, the type of loaded drug, the drug loading amount and location, providing a versatile platform and allowing the formulators to finely balance the release performance of drugs intended for oral administration. Overall, the study demonstrates that hybrid, solvent-free b-MPs produced by spray congealing are an extremely versatile delivery platform able to efficiently encapsulate and release very different types of drug compounds.

1. Introduction

Microparticles (MPs) have been introduced since the early 1990s as multi-unit dosage form for the oral delivery of active pharmaceutical ingredients (APIs) [1-3]. From their early development, MPs composed either by lipids or polymers have been developed in order to modulate the release of various APIs. Polymeric MPs have been produced using a wide range of different natural, semi-synthetic and synthetic polymers [4]. The possibility to achieve a controlled drug release by polymeric MPs relies on their bio-degradation, which in turns depends on polymer properties such as monomer composition, molecular weight and glass transition temperature [5]. By contrast, lipid excipients are natural-derived ingredients that can be digested by lipases to form smaller absorbable components (e.g. glycerol, fatty acids). Lipid ingredients are highly versatile in terms of structure (they can be either completely non polar, polar but insoluble or water-soluble) [6,7] and their properties are mainly influenced by the degree of unsaturation in fatty acids, the fatty acid chain length and type/number of ester functions. Solid formulations produced using insoluble lipid excipients can prolong the release of drugs by controlling the ingress of water through the lipid matrix (diffusion-based mechanism) as well as by enzymatic digestion or lipolysis (erosion-based mechanism) [8].

With the evolution of microscale particle engineering, the possibility to combine lipids and polymers in single multiparticulate drug delivery systems has attracted particular attention in the last few years [9-12]. The diversified combination of materials of different nature to produce hybrid MPs can potentially equip the delivery platform with new properties and unprecedented control over the drug release performances. Specifically, the development of hybrid MPs allows to selectively merge the advantages of both excipients with the ultimate goal of

* Corresponding author.
E-mail address: beatrice.albertini@unibo.it (B. Albertini).

https://doi.org/10.1016/j.ejpb.2023.07.017
Received 7 June 2023; Received in revised form 25 July 2023; Accepted 28 July 2023
Available online 28 July 2023

achieving precise control over drug release profiles. Most methods for the preparation of hybrid MPs involve the preparation of multiple emulsions followed by spray drying [11,13,14] or, more recently, microfluidic-based methods [15]. The production of such system, however, is based on complex protocols involving multiple steps [11], the use of solvents (e.g. acetone, dichloromethane, ethyl acetate) [10-13], poor process yields [16] and/or low encapsulation efficiencies (generally lower than 50%) of active molecules [11]. Consequently, it is desirable to design a novel polymer–lipid hybrid platform without these associated issues.

In this contest, we have recently developed a solvent-free process based on spray congealing technology that enabled the fabrication of a new type of hybrid biphasic microparticles (b-MPs) [17]. Spray congealing, also known as spray cooling or spray chilling, is based on the atomization and solidification of a molten material sprayed in a cooling chamber without use of solvents [18,19]. After a screening of various lipids, surfactants and hydrophilic carriers, selected water-in-oil non-aqueous emulsions were transformed by spray congealing into solid particles containing a fluorescent dye [17]. The particle size of b-MPs, ranging 100–500 μm, excluded their use for systemic drug delivery by parenteral, inhalation or transdermal routes. Nevertheless, their properties (non-aggregated, spherical and free-flowing) makes them suitable for oral delivery applications. Depending on the composition of the lipid (external) and polymeric (internal) phases, b-MPs with different architectures were successfully produced, including particles with homogeneous structure as well as "multicores-shell" particles. In contrast to the aforementioned methods used for hybrid b-MPs preparation, the proposed manufacturing technique can boast a green approach, ease of production and potential scalability, with great potential application in the pharmaceutical industry. Nevertheless, the encapsulation and release behavior of APIs in such novel b-MPs have never been investigated.

The loading of an API into a dosage form can affect the production process outcome as well as the structural and morphological properties of the produced delivery system. This is particularly relevant when dealing with complex delivery platforms, such as biphasic systems. Moreover, variables including API molecular properties, loading amount, location (e.g. either in the inner or outer phase of the particle) could affect both the structure of the b-MPs, the encapsulation efficiency and the performance of drug release [20].

Therefore, in this work we have investigated the potential of this innovative hybrid microparticulate system for the oral delivery of various APIs. Specifically, the investigated hybrid MPs are composed of Compritol 888 ATO as the main lipid carrier, whereas polyethylene glycol (PEG 400) is used as polymeric core material. Three orally delivered APIs covering a wide range of hydrophobicity were selected as model drug compounds: Fluconazole (FLU), Tolbutamide (TBM) and Nimesulide (NIM). As shown in Table 1, they differ from logP, crystalline equilibrium solubility, which values were measured experimentally in suitable aqueous media (pH selected as to have the drug molecule in non-ionised form) and BCS classification. This would allow to evaluate the ability of hybrid microparticles to efficiently encapsulate drugs with very different hydrophobic/hydrophilic properties and to compare their release profiles. Hybrid b-MPs loaded with the three compounds were produced and characterized regarding size, morphology and physical state. The influence of API type and amount on the external and internal structures was investigated by means of various microscopy-based techniques (HSM, SEM and Raman imaging) with a specific attention on possible alterations of the lipid-polymer interface and modifications in the distribution of the two phases. To investigate the suitability of hybrid b-MPs as oral drug delivery platform, encapsulation efficiency and *in vitro* release profiles achieved by hybrid b-MPs were evaluated and compared with those obtained with traditional one-phase lipid MPs.

Table 1
Properties of APIs used in this study.

APIs	Solvent used for solubility and dissolution studies	Solubility at 37 °C (μg/ml)[a]	Log P	BCS class
Fluconazole	Water	6216.9 ± 412.0	0.5[b]	I
Tolbutamide	NaCl/HCl buffer (0.2 M, pH 1.2)	106.9 ± 15.9	2.13[c]	II
Nimesulide	NaCl/HCl buffer (0.2 M, pH 1.2)	8.9 ± 0.3	3.08[c]	II

[a] Experimental values; [b] from [21]; [c] from[22].

2. Material and methods

2.1. Materials

Compritol®888 ATO was kindly supplied from Gattefossè (Milan, Italy). Cetylstearyl alcohol, polyethylene glycol (PEG) 400, tolbutamide (TBM), nimesulide (NIM) were purchased from Sigma Aldrich (Steinheim, Germany). Fluconazole (FLU) was obtained from Acofarma (Madrid, Spain). Rhodamine, used as coloured dye for the PEG phase, was purchased from Sigma Aldrich. All other chemicals were of analytical grade. The properties of the APIs used are reported in Table 1.

2.2. Preparation of MPs

Spray congealing was employed to obtain solid MPs, as schematized in Fig. 1. The spray congealing apparatus comprises a feeding tank, an atomizer and a cooling chamber. An external-mix two-fluid atomizer, called Wide Pneumatic Nozzle (WPN), was used. Emulsions (5 g) were prepared as previously reported [17]. Briefly, the hydrophobic phase, consisting on a lipid (Compritol®888 ATO) and of a hydrophobic surfactant (cetylstearyl alcohol) at 3:1 ratio, was heated at 70 °C until melting. The hydrophilic phase (PEG 400 alone or with surfactant Cremophor EL) was heated at the same temperature (70 °C), added to the lipid phase and gently mixed (250 rpm) via a magnetic bar keeping the temperatures at 70 °C using a hot stirring plate for at least 1 min. Then, the hot emulsions were introduced into the feeding tank of the spray congealing apparatus. All emulsions (Table 2) were atomized at 1.5 bar air pressure and nozzle temperature of 70 °C. The atomized molten droplets solidified in the cooling chamber at room temperature (25 °C), allowing the formation of solid particles. MPs were collected from the bottom of the cooling chamber and stored in polyethylene closed bottles at 25 °C. The percentage yield was calculated using the following Equation:

$$\text{Yield} = (\text{Amount of recovered MPs (g)})/(\text{Amount of emulsion (g)}) \times 100$$

For the preparation of drug-loaded b-MPs, 2% w/w of each API extra-formulation was solubilized into the hydrophilic phase prior to emulsion formation. In addition, lipid microparticles (L-MPs) consisting only of the main lipid (Compritol®888ATO) were prepared.

2.3. Interfacial tension measurements

The interfacial tension (IRT) between the hydrophilic and lipophilic phases was measured by a tensiometer (Kruss tensiometer K8600, Hamburg, Germany) with the Du Noüy ring method, similarly to previously reported studies [17,23]. First, the accuracy of the platinum-iridium ring was validated by determining the surface tension of water (72 mN/m). For these measurements, 4 mL of lipid-PEG emulsions were transferred in a glass vessel which was thermostated at 70 °C by a water bath. The emulsion was then left without agitation until two separate phases formed: the upper lipid-rich phase and the bottom PEG-rich phase. The interfacial tension at the two phases interface was then measured. Measurements were repeated six times for each sample and the mean ± SD was calculated.

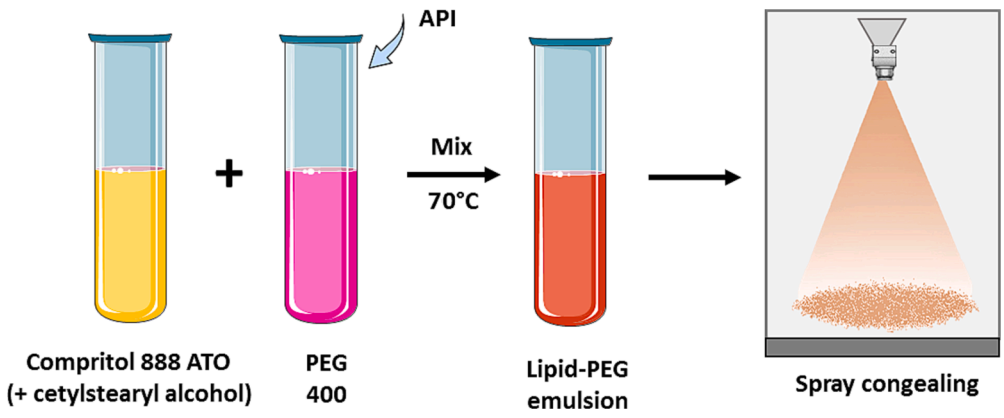

Fig. 1. Schematic Illustration of the fabrication process of the drug-loaded b-MPs.

Table 2
Composition of the three batches of the hybrid b-MPs (b-MPs1 and b-MPs2) and one phase L-MPs produced by spray congealing.

Formulation	Composition (% w/w)				
	Compritol 888 ATO	Cetylstearyl alcohol	PEG 400	Cremophor EL	API *
b-MPs1	60	20	20	–	2
b-MPs2	60	20	15	5	2
L-MPs	100	–	–	–	2

* The API was added at 2% w/w extra-formulation.

2.4. Particle size analysis

Size distribution of b-MPs was evaluated by sieve analysis using a vibrating shaker (Octagon Digital, Endecotts, London, UK) and a set of six sieves ranging from 50 to 500 μm (Scientific Instrument, Milan, Italy).

2.5. Optical microscopy

Hybrid b-MPs were observed under optical microscope using a Nikon Eclipse E400. Glass slides containing 10–20 mg of MPs were firstly observed at 25 °C. Then, they were heated by a hot stage apparatus (Mettler-Toledo S.p.A., Novate Milanese, Italy) to 70 °C to allow the melting of the solid MPs. Melting was required in order to visualize the two phases (polymeric and lipid) by optical microscopy, otherwise only the external surface could be appreciated. Thus, images were taken at 70 °C using a Nikon Digital Net Camera DN100 connected to the microscope at a magnification of 10 ×.

2.6. Scanning electron microscopy (SEM)

The shape and surface morphology of hybrid b-MPs and one phase L-MPs were evaluated by scanning electron microscopy (SEM). Samples were fixed on the sample holder with double-sided adhesive tape and examined by means of a scanning electron microscope (Zeiss Scanning Electron Microscope Model EVO 50 EP) operating in low-vacuum mode (90 Pa) at 10.0 kV accelerating voltage.

2.7. Differential scanning calorimetry (DSC)

DSC analysis was performed with a Perkin-Elmer DSC 6 (Perkin Elmer, Beaconsfield, UK). Before measurements, the instrument was calibrated with indium and lead for the temperature, and with indium for the enthalpy. Samples (5–10 mg) of MPs were placed into aluminum pans and analyzed by DSC under a nitrogen flow of 20 mL/min. After 1 min at 30 °C the samples were heated from 30 to 90 °C at a heating rate of 10 °C/min.

2.8. Confocal Raman mapping (CRM)

A WITec Alpha 300 Raman spectrometer was used to generate Raman spectra of the samples in the range of 0–3600 cm-1, with a spectral resolution of 3 cm-1. Raman spectrometer was connected with a confocal microscope, equipped with TrueSurface attachment and EMCCD detector for ultra fast and sensitive imaging. The samples were irradiated with a focused laser beam at a power of 15 mW. The laser was emitting at the wavelength of 532 nm. Measurements were performed using an air objective with a magnification of 20x and a numerical aperture (NA) = 0.4. The microparticles were mapped with a spacial resolution of 3 μm. The measuring step was set to 1 μm, the accumulation time of a single spectrum was 0.5 s. The Raman maps were recorded for microparticles which diameter did not exceed 100 μm.

Before Raman mapping, Raman spectra for all raw materials were recorded in order to identify key marker bands for identification of API (TBM) and excipients in five batches of MPs. The collected Raman mapping data was analyzed by means of the Project FIVE 5.3 software. The analysis based on the calculation of the integral value (area under the band) for the selected bands as well as chemometric analysis (k-means cluster analysis) were performed in order to describe a distribution of the two phases in the hybrid b-MPs well as the drug substance within the MPs.

2.9. Quantification of APIs encapsulation efficiency

Drug loading into b-MPs was determined by adding 5 mg of b-MPs in 5 mL of distilled water, heated to 70 °C to melt the solid carrier and centrifuged. The amount of APIs in the supernatant was detected by measuring their absorbance with a Cary 60 UV–Vis spectrometer (Agilent Technologies GmbH, Waldbronn, Germany) at 251, 227 and 298 nm for FLU, TBM and NIM, respectively. Drug loading (DL %) and Encapsulation efficiency (EE %) were calculated as:

$$\text{Drug loading (\%)} = (\text{drug (mg)})/((\text{drug} + \text{carrier})(\text{mg})) \times 100$$

$$\text{EE (\%)} = (\text{drug (mg)})/((\text{theoretic drug (mg)}) \times 100$$

2.10. Determination of APIs equilibrium solubility

Solubility measurements at equilibrium of APIs, loaded MPs, and Phy mix were performed at 37 °C. An excess of crystalline API was added to 10 mL of the respective medium (purified water for FLU, solution at pH 1.2 for TBM and NIM). The samples were magnetically stirred for 48 h, equilibrated for 2 h, and the suspensions were then centrifuged at

10.000 rpm for 10 min. The supernatant was filtered through a 0.20 μm Nylon membrane filter. The filtrates were suitably diluted with the same solvents and analyzed by UV–Visible spectrophotometer at 251, 227 and 298 nm for FLU, TBM and NIM, respectively. Each sample was analyzed at least in triplicate.

2.11. In vitro study of drug release from MPs

Being a BCS class I API, FLU release form MPs was studied using *sink* conditions, whereas *non-sink* conditions were used for the two BCS class II drugs (TBM and NIM). A suitable amount of MPs was added to 500 mL of dissolution medium (see Table 1) kept at 37 °C using the Apparatus 2 (paddle apparatus) of the Eur. Ph. (DT 800 Erweka GmbH, Heusenstamm, Germany) rotating at 50 rpm. 200 mg of FLU-loaded MPs were used, resulting in a drug concentration of 8 μg/ml, while in case of NIM, 400 mg of MPs were used, resulting in a drug concentration of 16 μg/ml. In case of TBM-loaded MPs, a smaller-scale dissolution system was used, consisting in 37 °C thermostated glass vial containing 40 mL of dissolution medium (see Table 1) and 300 or 540 mg of MPs were used in order to achieve the desired *non-sink* conditions (drug concentration of 150 μg/ml or 270 μg/ml). At specific time points, 1 mL of the medium were withdrawn using an 8 μm filter to avoid the removal of the MPs and replaced with fresh medium. The amount of drug was determined spectrophotometrically at 251, 227 and 298 nm for FLU, TBM and NIM, respectively. The main size fraction of MPs, corresponding to 250–355 μm, was used for all samples. The results were expressed as drug released percentage (%) or concentration (μg/ml) in function of time. At least three replicates were analyzed for each formulation.

Following release studies of TBM-loaded MPs, samples of the dissolution medium were analyzed by dynamic light scattering (DLS) to check for the presence of colloidal species (i.e. micelles) against a blank of fresh dissolution medium. A Brookhaven 90-PLUS instrument (Brookhaven Instruments Corp., Holtsville, NY, USA) with an He-Ne laser beam at a wavelength of 532 nm (scattering angle of 90°) was used for measurements.

2.12. Statistical analysis

Two-ways analysis of variance (ANOVA) followed by the Bonferroni posthoc test (GraphPadPrism, GraphPad software, Inc., San Diego, CA, USA) was used.

3. Results and discussion

3.1. Production and characterization of hybrid b-MPs loaded with different APIs

Hybrid microparticles were produced following a method previously reported [17]. This process can be divided in two steps, as illustrated in Fig. 1. In the first step, a hot "W/O-like" emulsion consisting in PEG 400 as dispersed phase and molten lipid mixture (Compritol and cetylstearyl alcohol) as continuous phase was prepared under continuous stirring and keeping the temperature at 70 °C. In the second step, the emulsion was sprayed by means of the spray congealing apparatus equipped with the WPN atomizer [24]. FLU, TBM and NIM were chosen as representative drug compounds and were loaded at 2% w/w into b-MPs by dissolving them into the PEG phase. Preliminary studies were performed prior to b-MPs production to ascertain the solubility of the selected drugs in PEG 400. All three compounds were freely soluble in PEG (solubility at 25 °C in the range 100–250 mg/ml), confirming the ability of PEG of dissolving a wide range of compounds [25].

The spray congealing process resulted in the formation of solid and free-flowing microspheres. The process is fast, simple, solvent-free and the process yields ranged 70–80% for batches of 5 g size.

The particle size of spray congealed MPs indicated a Gaussian distribution, with the majority of particles in the range 100–500 μm. As example, the particle size distribution of the TBM-loaded formulations is shown in Fig. 2A, while the particle size analysis of MPs loaded with FLU and NIM is reported in Fig. S1A and Fig. S2A, respectively. The particle size was not influenced by the type of loaded drug, as the distributions were similar between the batches loaded with the three APIs as well as to the unloaded MPs (Fig. S3A). Slight differences were observed between hybrid b-MPs and one-phase L-MPs. The latter showed a broader distribution with presence of MPs either very small (<100 μm) or large (>500 μm) with lower amount of MPs with intermediate diameter. However, the mean particle size were about 350–400 μm for all batches (Table S1). As >40% of b-MPs had diameter between 200 and 355 μm, this size fraction was used for further studies.

Shape and surface morphology of b-MPs were evaluated by SEM. As example, a SEM micrographs of b-MPs1 loaded with TBM, FLU and NIM are shown in Fig. 2B, Fig. S1B and Fig. S2B. All batches showed highly spherical particles without holes or cracks on the surface and no differences were observed between loaded and unloaded b-MPs (Fig. S3B).

Following production, b-MPs were studied by HSM in order to understand the effect of drug on the shape, size and distribution of the PEG cores into the lipid matrix. As the lipid matrix melts at about 65 °C, the lipid/PEG interfaces could be clearly detected by keeping the samples at 70 °C (Fig. 3A). Unloaded b-MPs1 clearly show the inner polymeric phase consisted in large PEG droplets (with diameters up to 30 μm) while more uniform systems with undistinguished inner phase were observed in case of unloaded b-MPs2. These results are consistent with the earlier research on Rho-loaded b-MPs with the same composition. Comparing the structure of drug-loaded b-MPs with the unloaded systems (Fig. 3A), the type of drug did not seem to have a substantial influence on the internal structure of b-MPs1 as the morphology of the molten emulsions were quite homogeneous. Nevertheless, in case of drug-loaded b-MPs2, numerous and small PEG droplets of few μm diameters appeared in the drug-loaded systems. Among the three APIs, biphasic systems containing FLU seemed to originate slightly smaller droplets than those with the other two drugs. Thus, HSM analysis showed that the presence of drug molecules can affect the interactions at the lipid/PEG interface (e.g. PEG and surfactants distribution). Therefore, the effect of drugs on the emulsion properties was studied by measuring the interfacial tension, σ, between lipid and PEG phases.

Lipid-PEG emulsions, if kept without agitation at 70 °C, undergo phase separation (Fig. 3B), making possible to measure the interfacial tension between the two phases. The results, reported in Fig. 3C, showed that the presence of drugs influenced the lipid/PEG interface. For the binary system composed only of Compritol as lipid and PEG, for example, the measured values of σ decrease when drugs were dissolved in PEG phase from 4.50 ± 0.50 N/m in the absence of drugs to 3.00 ± 0.29 N/m, 3.55 ± 0.23 N/m and 3.17 ± 0.26 N/m for FLU, TBM and NIM, respectively. The same tendency, but with lower values of σ, was observed for the emulsions containing a lipid phase composed of Compritol and cetylstearyl alcohol (corresponding to the formulation of hybrid b-MPs1). The third emulsion type investigated, corresponding to the composition of b-MPs2 and characterized by the presence of 5% w/w of surfactant Cremophor EL, presented very low values of σ, below the sensitivity of the instrument. Therefore, for this formulation it was not possible to discriminate among the influence of the three APIs. Notably, FLU was the drug that most behave like a "surface active" agent, determining the highest decrease of σ in both emulsion types ($p < 0.01$ and $p < 0.05$). This result is consistent with the structure of b-MPs observed in Fig. 3A, where FLU-containing particles presented the smallest and more homogeneous droplets size among the three model APIs. The effect of TBM was similar to FLU in the PEG/Compritol biphasic system, but less evident in the biphasic system containing cetylstearyl alcohol and finally the impact of TBM on the interfacial tension was negligible for both systems as the values of σ were not statistically different from the emulsion without APIs ($p > 0.05$). This can be explained by considering the log P value of FLU (log P is about 0 meaning that this compound is equally partitioned between the

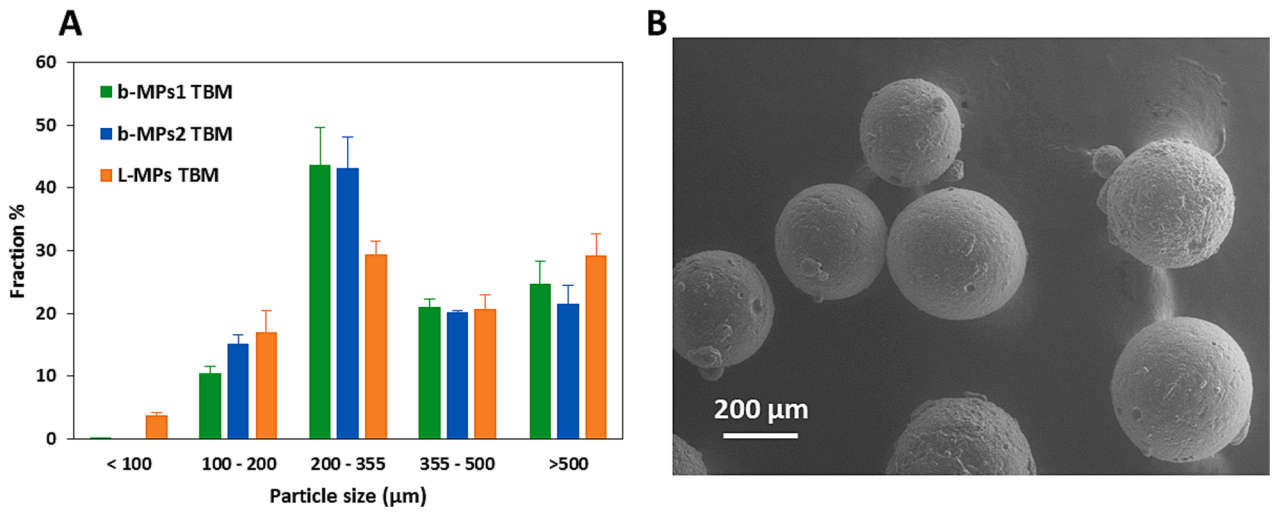

Fig. 2. (A) Particle size distribution of hybrid (b-MPs1 and b-MPs2) and L-MPs containing TBM (n = 3). (B) Shape and surface morphology of hybrid b-MPs1 containing TBM investigated by SEM.

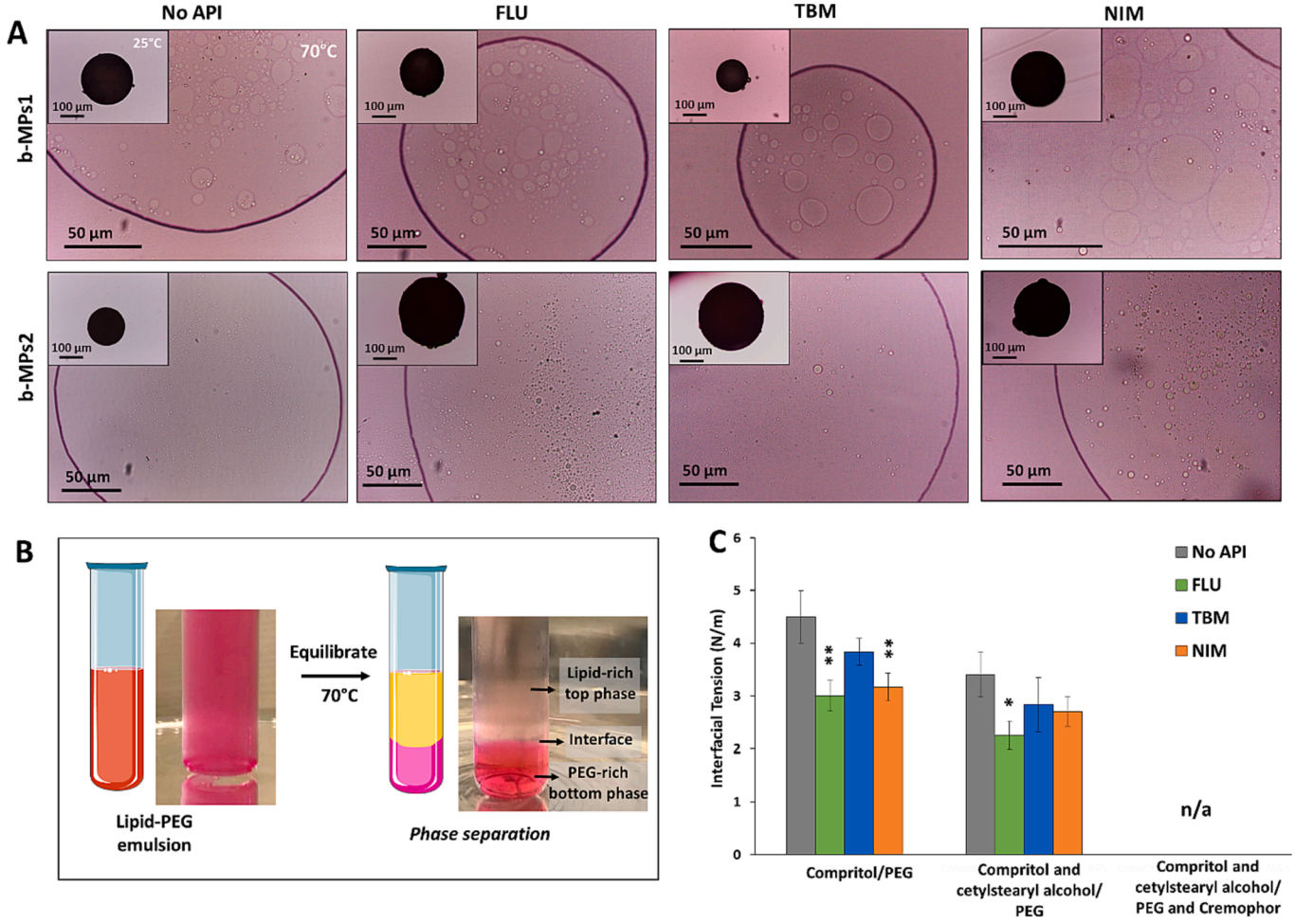

Fig. 3. (A) Hot Stage Microscopy images of hybrid b-MPs1 and b-MPs2 containing FLU, TBM and NIM. Images of solid particles were depicted at room temperature (25 °C) while the distribution of the lipid/PEG phases was observed after melting (70 °C). (B) Evolution with time of hot lipid-PEG emulsions. A colored dye (rhodamine) was added to the hydrophilic phase to provide a better visualization of the two phases. (C) Interfacial tension measurements of various lipid-PEG emulsions without and with three model drugs dissolved at 2% w/w into the PEG phase. Data represent mean ± S.D. (n = 6), the level of significance was set at the probabilities of * $p < 0.05$, ** $p < 0.01$, *** $p < 0.001$ with respect to the corresponding sample without API. n/a indicates that the values were below the limit of detection of the instrument.

octanol and the aqueous phases) which indicate a good affinity for both polar hydrophilic as well as for non-polar hydrophobic solvents. Moreover, the formation of strong hydrogen bonds with its solvents has been reported as the most important mechanism determining FLU solubility [26]. Therefore, hydrogen bonding with both the PEG phase (with the ether oxygen atoms on the backbone chain) and the lipid phase (with the hydroxyl groups of the mono- and di-glycerides of Compritol and of cetyl stearyl alcohol) might also explain the observed surface properties.

Overall, the three APIs have shown to influence the surface properties of the PEG/lipid emulsions at various extent, thus it can be hypothesized that APIs localized, in whole or in part, in the interfacial region between the two phases, thus decreasing the interfacial tension.

3.2. Drug loading and release behavior from hybrid b-MPs

The potential of hybrid b-MPs for encapsulation and controlled release of the various model APIs was investigated.

Table 3 reports the results regarding the efficiency of b-MPs in encapsulating the active molecules as compared to one-phase L-MPs. L-MPs showed variable drug loading (DL) values for the three compounds, and specifically the encapsulation efficiency (EE) was very good (higher than 93%) for TBM and NIM, but slightly lower (86.1%) for FLU, the less lipophilic molecule among the three. This is a very typical issue when a hydrophilic cargo has to be loaded into a lipid formulation due to the different nature of the two materials. It is noteworthy that by using spray congealing, a good encapsulation was achieved even with FLU. As regard the hybrid systems, the EE % ranged 90.5–92.7% for b-MPs1 and even higher (93.4–99.6%) for b-MPs2. Specifically, the loading amount achieved by b-MPs1 was statistically different compared to L-MPs for FLU and TBM, but not for NIM. Differently, the difference in the loaded drug in b-MPs2 compared to L-MPs was observed for all APIs, even though with various levels of significance (see *p*-values Table 3).

Overall, the encapsulation of drugs into b-MPs was more consistent among the different batches compared to L-MPs, and the DL values were all close to 2%. The statistical analysis of the encapsulation performance of each type of MPs regard the three different APIs confirmed that the hybrid formulations could equally load all APIs without significant differences ($p > 0.05$) whereas a significant difference was obtained for L-MPs ($p < 0.001$). This demonstrates the superior ability of b-MPs in encapsulating compounds having very different hydrophilic/lipophilic characteristics, as long as the loaded amount can be solubilized into the inner PEG phase.

Drug release profiles obtained from the MPs loaded with the three drugs in suitable dissolution media are depicted in Fig. 4.

Being classified as BCS class I and having a pH-independent solubility, the release of FLU was studied in water under *sink conditions U* (Fig. 4A). As expected, the dissolution of free drug was immediate (100% FLU dissolved within 1 min). A very fast drug release was observed also using b-MPs2, with 95% of drug released after 15 min and 100% after 30 min. Hybrid b-MPs1, by contrast, behaved similarly to L-MPs and a sustained drug release with minimum burst release was observed. This gradual and prolonged release after exposure to dissolution medium can be attributed to a diffusion-based release mechanism of the drug through the lipid matrix. Differently, an immediate release profile was observed in case of b-MPs2, probably due to the presence of 5% w/w surfactant (Cremophor EL) in the formulation. This component can act as wetting agent, promoting the diffusion of water medium within the lipid particles.

As TBM and NIM are both BCS class II drugs with acidic character, dissolution tests were performed under *non-sink conditions* using buffer pH 1.2 in order to have the molecules in the un-ionized forms. The dissolutions of free drugs were slow and after 6 h only the TBM concentration in the dissolution media approached its solubility limit, indicated by the dotted line (Fig. 4B), while NIM dissolution was lower than its equilibrium solubility value (Fig. 4C). One-phase L-MPs further reduced the drug release, determining a slow and incomplete release of TBM and NIM, as most drugs were not released within 6 h. Conversely, the release profiles observed for hybrid b-MPs were quite different for the two drug compounds. In case of TBM, the release behavior from b-MPs1 and b-MPs2 was quite unexpected and characterized by two main phases: a fast release in the first hour that reaches the TBM solubility limit, followed by a second phase of extended drug release in which the drug concentration exceeded its solubility threshold (Fig. 4B). A different behavior was observed in case of NIM-loaded b-MPs, where a modest increase in the release speed was observed passing from L-MPs to b-MPs1 and further from b-MPs1 to b-MPs2, but the drug release remained below its solubility (Fig. 4C).

Overall, the difference in release performance between hybrid b-MPs and one-phase L-MPs is not significant (except for the introduction of the surfactant in the formulation) for FLU, indicating that controlled drug release can be obtained both by encapsulating the drug into the lipid matrix either as powder and solubilizing the API into the PEG phase, indifferently. Differences between dissolution profiles from one-phase and hybrid b-MPs raised increasing the drug hydrophobicity. In case of TBM and NIM, in fact, the dissolution performances of b-MPs were quite different from those of L-MPs. The limited improvement in dissolution of b-MPs containing NIM compared to TBM might depend on its higher logP value as well as on the very low solubility value of this drug, which is one order of magnitude lower compared to that of TBM (Table 1). Being a highly hydrophobic drug, NIM has a strong tendency to precipitate as soon as the NIM-PEG solution is diluted with the aqueous buffer. Thus, it is likely that a situation of dynamic equilibrium is established at the interface of the MPs during dissolution involving two opposite processes: drug dissolution and drug precipitation. The presence of a surfactant (Cremophor EL) would favor the dissolution process in spite of the precipitation one, thus determining a better performance (b-MPs-2 compared to b-MPs1). Additionally, the distribution and dimensions of the PEG pores in the lipid matrix can be an additional factor influencing the release profile. In fact, after initial wetting of the MPs surface, the water ingress into the lipid matrix leads to the progressive leaking of the drug/PEG phase, being water-miscible, into the dissolution medium. Thus, the presence of smaller numerous pores in b-MPs2 might facilitate the drug diffusion through more interconnected PEG channels compared to b-MPs1 with larger pores (Fig. 3A), as observed in case of FLU and NIM.

The effect observed for hybrid b-MPs loaded with TBM in Fig. 4B, which is the dissolution of more API than it would be possible considering its crystalline equilibrium solubility (i.e. thermodynamic equilibrium between an excess of crystalline and dissolved API), might depend on different reasons. In this context it is important to discriminate between two different concepts: solubilization and supersaturation (also

Table 3
Drug loading (DL %) and encapsulation efficiency (EE %) values measured for drug-loaded hybrid (b-MPs1 and b-MPs2) and lipid (L-MPs) microparticles with particle size 200–355 μm (n = 3). Statistical analysis (Bonferroni post-hoc test) comparing the drug loaded in the different types of MPs.

APIs	DL ± SD (% w/w) *(EE %)*			Bonferroni post-hoc test	
	b-MPs1	b-MPs2	L-MPs	Comparison	*p*-value
FLU	1.85 ± 0.02 *(92.7)*	1.92 ± 0.01 *(96.0)*	1.72 ± 0.05 *(86.1)*	b-MPs1 vs. b-MPs2	0.002
				b-MPs1 vs. L-MPs	0.002
				b-MPs2 vs. L-MPs	<0.001
TBM	1.84 ± 0.10 *(91.8)*	1.87 ± 0.08 *(93.4)*	2.18 ± 0.16 *(108.8)*	b-MPs1 vs. b-MPs2	0,374
				b-MPs1 vs. L-MPs	<0.001
				b-MPs2 vs. L-MPs	0,037
NIM	1.81 ± 0.03 *(90.5)*	1.99 ± 0.01 *(99.6)*	1.87 ± 0.06 *(93.7)*	b-MPs1 vs. b-MPs2	<0.001
				b-MPs1 vs. L-MPs	0,076
				b-MPs2 vs. L-MPs	0,012

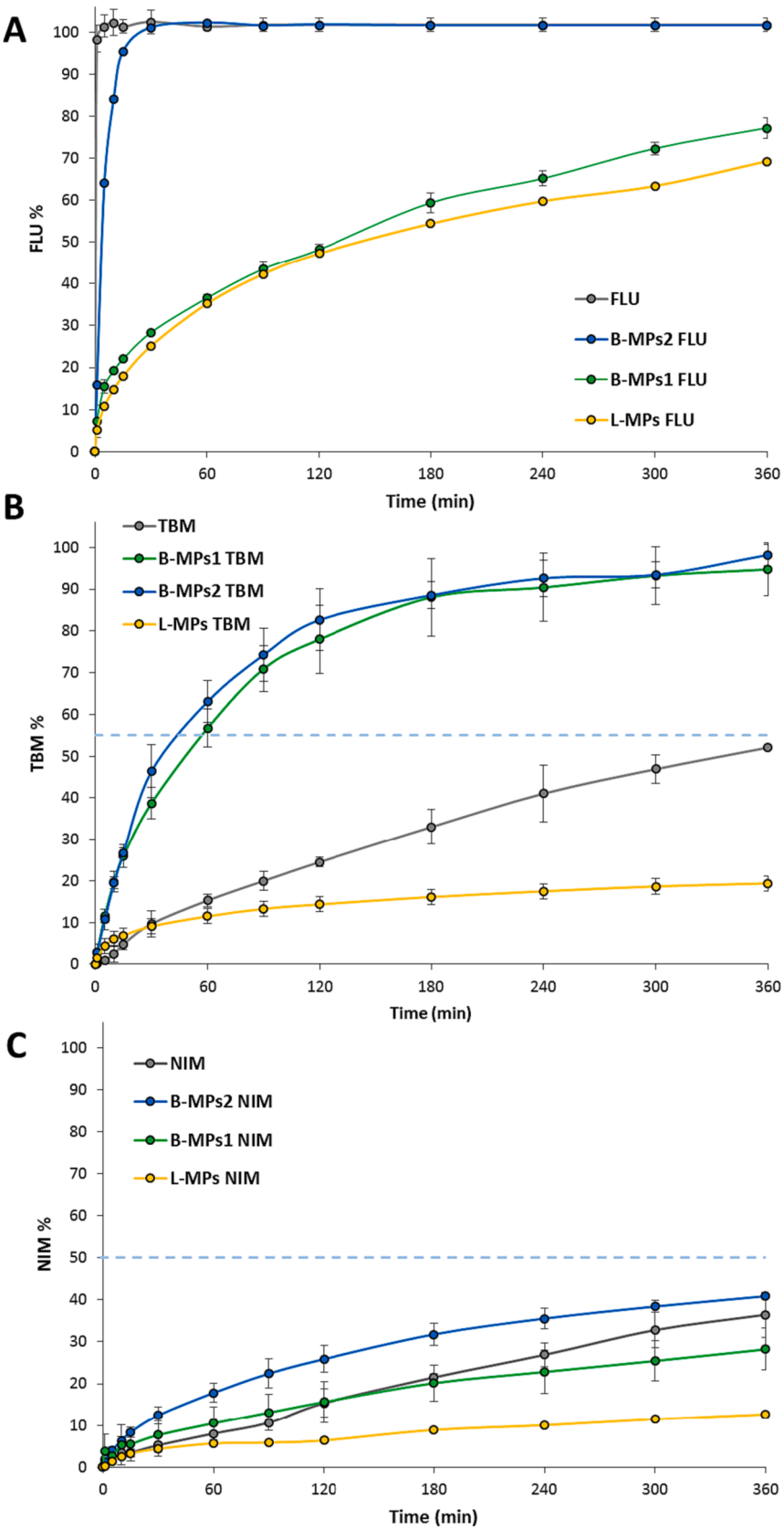

Fig. 4. Release profiles of fluconazole (A), tolbutamide (B) and nimesulide (C) from hybrid (b-MPs1 and b-MPs2) and lipid (L-MPs) microparticles with particle size 200–355 μm as well as release of pure drug (n = 3). In case of tests performed in non-sink conditions, the dashed line represents the equilibrium solubility of crystalline drugs in the same dissolution medium.

referred to as true supersaturation in literature) [27].

Solubilization refers to the increased drug apparent solubility due to the help of additional excipients, i.e. surface-active agents. Colloidal species (i.e. micelles) can, for example, formed in aqueous medium upon combination of amphiphilic components released by b-MPs2 (e.g. Cremophor EL). This first hypothesis was investigated by analyzing the dissolution medium by dynamic light scattering (DLS); however, no colloidal particles in the nanometer size range have been detected. Moreover, it has to be considered that b-MPs1, having no surfactant in the formulation, displayed the same behavior. Differently from solubilization, true supersaturation is a thermodynamically unstable state where drug molecules are molecularly dissolved in an aqueous solution at a concentration that exceeds the crystalline solubility. In contrast to pure TBM and L-MPs, where the drug is loaded as crystalline powder, in the hybrid b-MPs TBM is solubilized in the PEG phase. This means that the dilution of TBM, already molecularly dispersed in the PEG phase, into the aqueous medium is likely to determine a real supersaturation, similarly to the "spring" effect observed with amorphous solid dispersions [28]. It was interesting to note that the "supersaturated state" was kept for the test duration (5 h). PEG released in aqueous medium, which can act as co-solvent or as crystallization inhibitors, might account for this prolonged supersaturation. Nevertheless, the estimated PEG concentration in the dissolution medium, calculated considering the amount of particles and the dissolution volume, was moderate (about 1.3–1.8 mg/ml). Additional solubility studies performed in buffer solutions containing PEG within this concentration range (Fig. 5A) showed no significant variation with respect to TBM solubility value, confirming that TBM supersaturation is not related to the presence of PEG in the dissolution medium.

Another aspect to consider is the degree of supersaturation, that plays a key role on determining the duration of the supersaturated state: the highest the levels of supersaturation, the fastest the drug precipitation and the return to a thermodynamically stable state. Thus, to better investigate this behavior, additional release studies were performed changing the achievable supersaturation of TBM by varying the sink index (SI) [29]. SI was introduced by Sun et al.[30] to quantify the extent of "non-sinkness" of a dissolution test for supersaturating formulations and is defined as follows:

$$SI = \frac{Cs}{\frac{Dose}{V}}$$

where Cs is the solubility of crystalline drug, V the volume of dissolution medium, and Dose the total amount of drug in the test sample. Low SI values indicate high deviation from perfect *sink conditions* (corresponding to SI $\geq$ 3), defined as conditions where the "volume of dissolution medium that is at least 3–10 times the saturation volume" by the European Pharmacopoeia [31].

Fig. 5B shows the release profiles of b-MPs1 containing TBM performed at two SI values: the previous release profile performed at intermediate (SI = 0.7) non-sink condition was compared with dissolution at higher (SI = 0.4) non-sink conditions. The SI used affected the shape of the dissolution profiles. Passing from moderate to more significant *non-sink conditions*, we can observe that the concentration of TBM in the dissolution medium is higher and after 4 h TBM started re-crystallizing from supersaturated solution, as indicated by the red arrow. This result indicated the formation of a thermodynamically unstable state and confirmed the hypothesis of real supersaturation of TBM achieved by b-MPs. As an indicator of dissolution performance, we can consider the area under the curve (AUC), which is directly and inversely proportional to the dissolution and precipitation rates, respectively [32]. Although 100% release was not achieved using SI = 0.4, the dissolution profiles of b-MPs1 showed a good dissolution performance, i.e. high AUC (corresponded to the light blue area) and achieved a TBM maximum concentration that was almost two-times the drug equilibrium solubility. Moreover, the supersaturation state was maintained for about 4–5 h, which is considered a relevant time for determining an increase of drug absorption *in vivo*.

3.3. Variation of the loading amount and location of tolbutamide in hybrid b-MPs

Based on the interesting dissolution behavior of TBM-loaded b-MPs, we further investigated the possibility of loading higher TBM amounts in the PEG phase of b-MPs as well as of loading TBM in the external lipid compartment. To this aim, the formulation of hybrid b-MPs1 (Compritol 888 ATO and cetylstearyl alcohol as lipid phase, and 20 % w/w of PEG 400 as hydrophilic phase, see Table 1) was modified. Specifically, TBM loading into the hydrophilic phase (PEG) was increased from 2% (b-MPs@2H) of the previous formulation to 4% (b-MPs@4H) and 10% (b-MPs@10*H*) w/w. In addition, one batch was produced by loading TBM only in the lipid phase at 2% w/w (b-MPs@2L). One-phase lipid formulation containing 2% w/w of TBM (L-MPs) was evaluated as comparison. The composition of these batches is summarized in Table 4.

The particle size distribution and mean size of the obtained batches

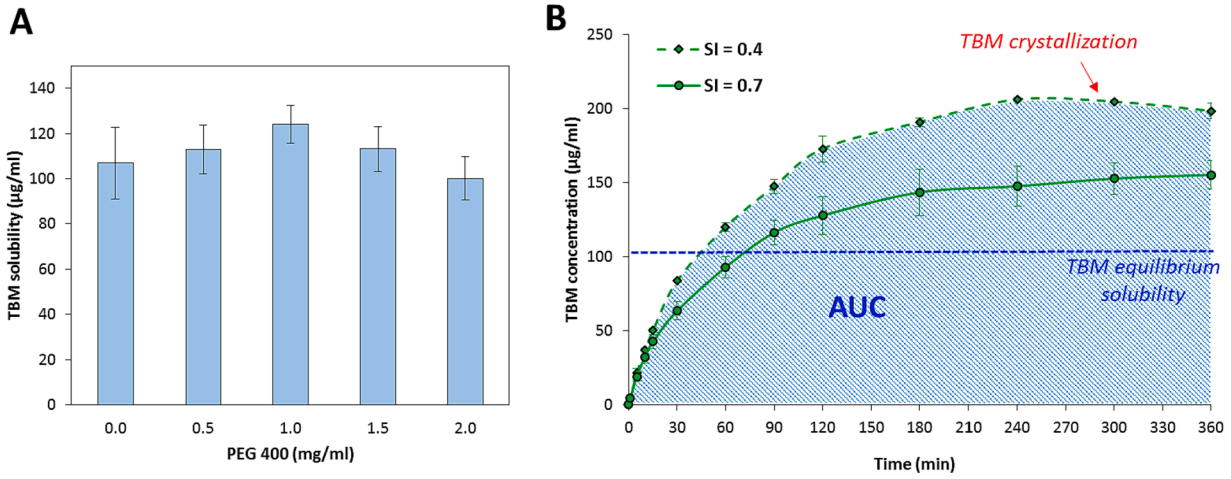

Fig. 5. A) TBM crystalline solubility in buffer pH 1.2 with increasing PEG amounts (n = 3). B) In vitro dissolution profiles of TBM from hybrid b-MPs under dissolution conditions with SI = 0.4 and SI = 0.7 in buffer pH 1.2 expressed as TBM concentration (µg/ml) in the dissolution medium at various times (n = 3). All samples had particle size 200–355 µm. The dashed blue line represents the equilibrium solubility of crystalline TBM in the same dissolution medium (C = 106.9 µg/ml). The area under the curve (AUC) is an indicator of dissolution performance. (For interpretation of the references to colour in this figure legend, the reader is referred to the web version of this article.)

Table 4
Drug loading (DL %) and encapsulation efficiency (EE %) values measured for hybrid (b-MPs1) and lipid (L-MPs) microparticles (particle size 200–355 μm) with TBM loaded at different amounts and locations (n = 3).

Formulation	TBM amount (% w/w)	TBM location	DL % (±SD)	EE %
b-MPs@2H	2	PEG phase	1.84 ± 0.10	91.8
b-MPs@4H	4	PEG phase	3.46 ± 0.11	86.4
b-MPs@10*H*	10	PEG phase	7.38 ± 0.07	73.8
b-MPs@2L	2	Lipid	1.97 ± 0.19	98.7
L-MPs	2	Lipid	2.18 ± 0.16	108.8

(Fig. S4 and Table S2) was not affected by varying the drug loading amount and location. The main particle size fraction was always in the range 200–355 μm, thus this size fraction was used for further studies.

The DL values of the MPs (Table 4) depended on the drug amount: the formulations with lower drug amount (2% w/w) allowed optimum drug encapsulation with EE values always higher than 91%, regardless of the TBM loading in the PEG phase or in the lipid phase of the b-MPs. The EE values decreased concurrently with the increasing of the TBM amount, probably due to the difficulty to completely dissolve the drug in PEG phase and to include this phase into the lipid matrix during the spray congealing process. Nevertheless, EE was still good with values above 73%.

Another important aspect concerns the physical state of the different phases present in the b-MPs after cooling, which can be impacted by spray congealing process [18]. Fig. 6 showed the DSC curves of the drug-loaded hybrid b-MPs and L-MPs compared to raw lipid excipients and to the TBM. Compritol® 888 ATO showed its main melting endotherm at 78 °C and a weak endothermic event occurring at 45–55 °C is related to the transformation of the pseudohexagonal subcell arrangement of hydrocarbon chains, namely sub-α, into true hexagonal (α) subcell. Cetylstearyl alcohol presented a double melting endotherm at about 50 °C and 61 °C.

All MPs showed a single melting peak at temperatures intermediate between those of the two lipid excipients composing the lipid phase, accordingly to what observed previously [17]. The specific melting temperatures were 67–68 °C and 71–72 °C for hybrid (b-MPs) and one-phase (L-MPs) systems, respectively. This indicated complete miscibility of Compritol and cetylstearyl alcohol in the lipid phase. Moreover, the presence of TBM did not affect the solid state of the MPs. As regard the thermal behavior of TBM, the stable polymorph Form I_L was observed to transform into Form I_H at about 40 °C with an associated enthalpy change (endothermic), followed by the melting of the Form I_H at 131 °C. Endothermic signals related to the TBM melting were detected in the MPs samples slightly moved to a lower temperature (123–124 °C) only for b-MPs@4H and b-MPs@10*H* (red arrows). This indicates that the drug loaded in these MPs, or at least part of it, is present as crystalline form. The absence of the TBM peak in the other samples is probably related to the low amount of loaded drug and/or to fact the TBM is the molecularly dispersed (as solution in the PEG phase).

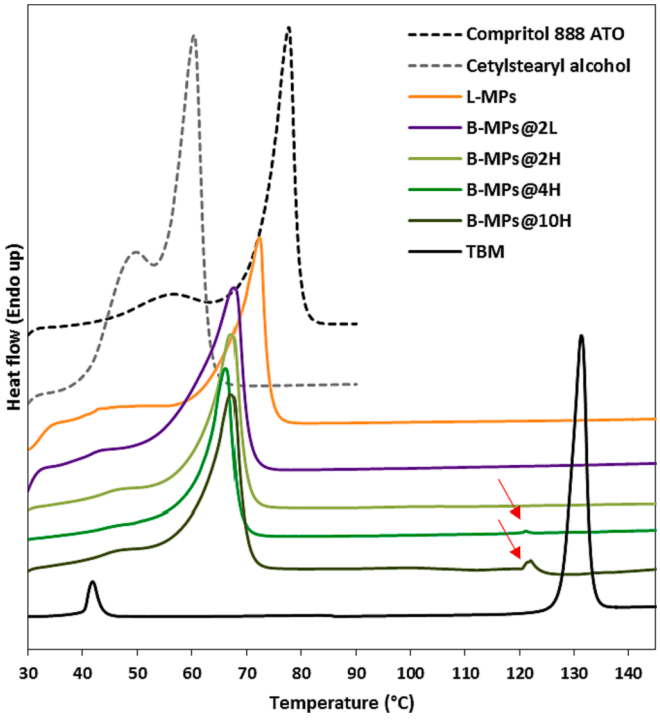

Fig. 6. DSC curves of MPs loaded with TBM at various amounts and locations, compared to the solid raw excipients (Compritol 888 ATO and cetylstearyl alcohol) and drug.

Similar information were gained by FT-IR analysis (Fig. S5), where weak signals of the drug were detected in the pattern of the MPs. Specifically, the characteristic band of TBM at 661 cm^{-1} was observed in all samples, but only in case of hybrid MPs having high drug amounts (b-MPs@4H and b-MPs@10*H*) it was possible to appreciate other characteristic bands of TBM at 1157, 1335 and 1702 cm^{-1}. Notably, these bands were markedly shifted compared to the values of pure TBM, suggesting a strong interaction with the PEG phase of the b-MPs. For example, the S=O symmetric stretching frequencies at 1335 cm^{-1} moved to 1340 cm^{-1} for b-MPs@10*H*, while the band at 1157 cm^{-1} related to the S=O asymmetric stretching moved to 1168 cm^{-1} and 1170 cm^{-1} in case of b-MPs@4H and b-MPs@10*H*, respectively. Moreover, FT-IR analysis allowed the clear identification of the PEG phase in the hybrid b-MPs due to its characteristic bands at 950, 1335, and the broad band at 1080–1140 cm^{-1}.

Overall, DSC and FT-IR analysis of TBM-loaded MPs indicate that the physical state of the MPs is maintained even by changing the amount and location of the loaded drug.

In order to detect how the loading of TBM might influence the MPs external and internal morphology, samples were investigated by means of SEM and confocal Raman mapping (CRM). CRM is the technique of choice for the structural characterization of MPs at the solid state as a powerful analytical option to identify the location of individual components within a multicomponent system.

Hybrid b-MPs prepared with TBM at various loading amounts/locations showed a spherical-like shape, as illustrated in Fig. 7. The surface of all TBM-loaded b-MPs was mainly smooth and uniform, similarly to unloaded hybrid b-MPs and to one-phase L-MPs. This indicates that the loading of TBM at various amounts/locations did not affect the particle external morphology.

Raman spectra registered for the TBM-loaded formulations as well as all raw materials (API and excipients) with key marker bands are presented in Fig. S6 and Fig. S7. The Raman signals registered at wavenumbers of 2886, 2852, 1452, 1302, 1138 and 1068 cm^{-1} are marker bands for lipophilic phase. The PEG phase can be identified by the signals registered at wavenumbers of 2889, 1478, 1290, 1141, 841 cm^{-1}. TBM can be identified by the key marker bands registered at wavenumbers of 3066, 1604, 1163, 1100, 815, 800 cm^{-1}.

Fig. 8 reports the results of CRM analysis of the five investigated formulations. Optical images of MPs are shown in the first raw. Raman maps obtained based on the integration of characteristic Raman bands (presented in the second row) did not allow for investigation of the spatial distribution of the various components in the MPs. Therefore, chemometrics was used to analyze Raman mapping data. The application of cluster analysis in the spectral range 770–980 cm^{-1} allowed for a differentiation of hydrophilic and lipophilic phase, as this wavenumber range was the most differentiating for PEG and lipid excipients in the Raman spectra. Whereas, in order to detect and identify TBM, the wavenumber range of 3030–3090 cm^{-1} was chosen because the drug present a clear and intensive band in this range. The colors of the

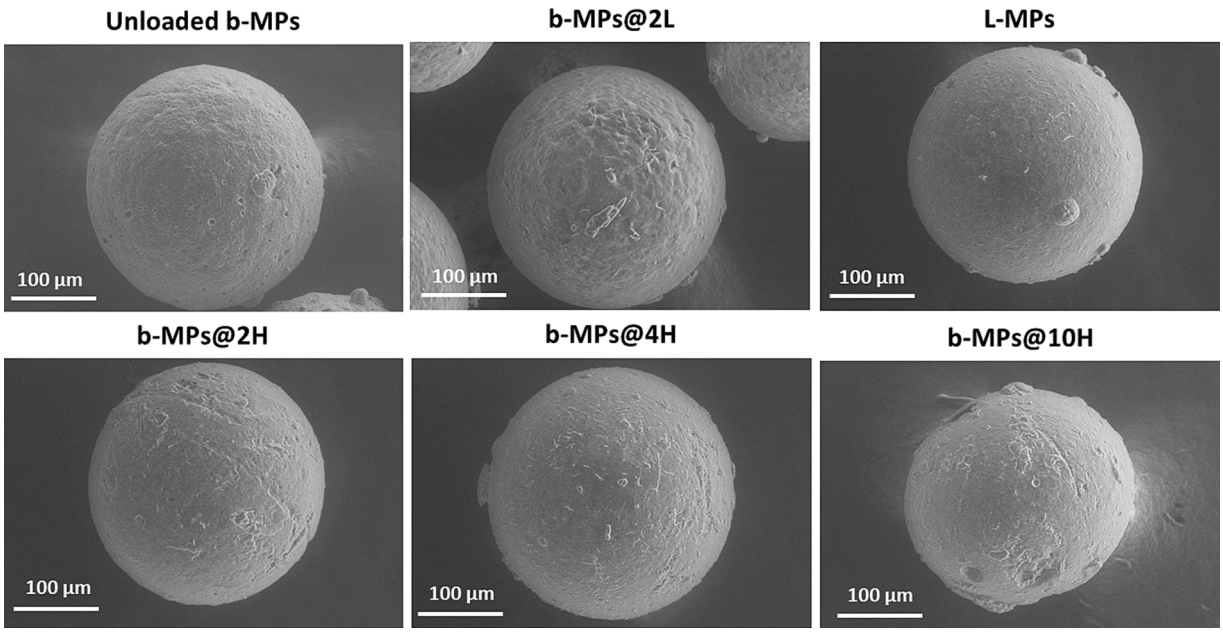

Fig. 7. SEM micrographs of hybrid particles loaded with TBM at various amount/locations (b-MPs@2H, b-MPs@4H, b-MPs@10*H* and b-MPs@2L) compared with unloaded b-MPs and one-phase lipid formulation containing 2% w/w of TBM (L-MPs).

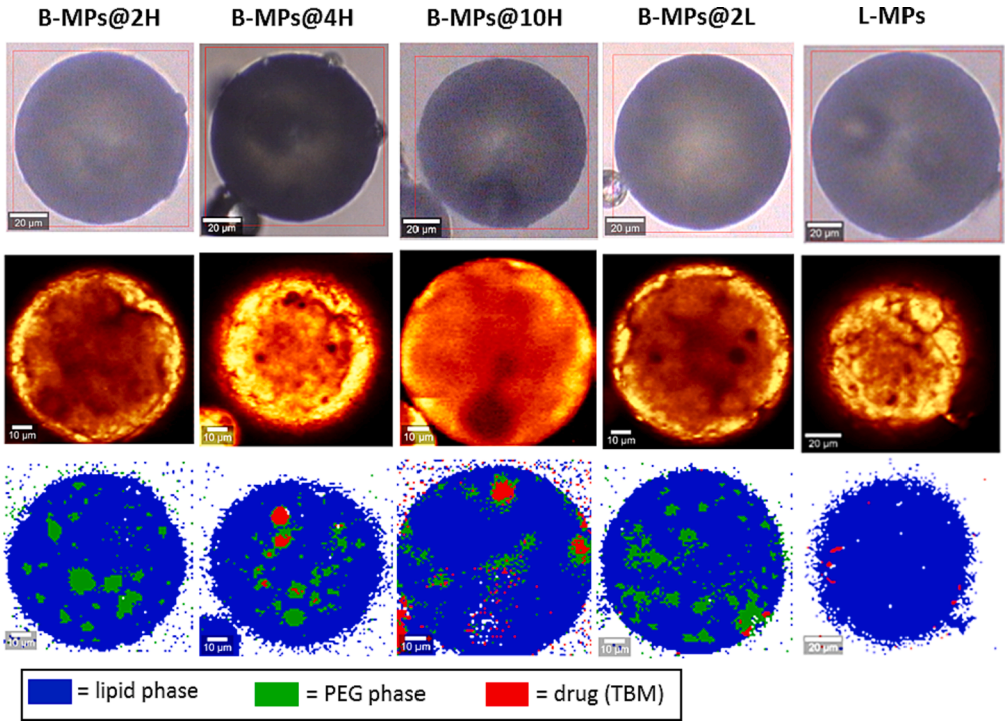

Fig. 8. Raman mapping images. The first row (at the top) shows visible pictures, the second row – Raman images obtained based on the integration of characteristic Raman bands at 2852 and 2886 cm-1; the third row – Raman images based on chemometrics (cluster analysis): lipid phase (blue area), PEG phase (green area) and TBM (red area). (For interpretation of the references to colour in this figure legend, the reader is referred to the web version of this article.)

resulting maps, shown in the third raw of Fig. 8 represent lipid phase (blue), PEG phase (green) and TBM (red). Differently to L-MPs, where only lipid matrix was detected, the PEG phase of hybrid b-MPs was clearly identified. All batches of hybrid b-MPs presented multiple PEG cores with size up to 10 µm into a crystalline lipid matrix.

Moreover, CRM analysis can help to understand how and in what form (crystalline or amorphous) the drug is distributed in the different phases of the MPs. The first consideration regards the drug loading amount, which is of critical importance as lower drug amount in the sample would lead to lower Raman signals. Indeed, only minor Raman signals of TBM were detected in the formulations with the lowest drug loading (2% w/w), whereas more defined TBM areas were observed in hybrid formulations with drug loaded at 4% and 10% w/w. Moreover, considering the formulations with equal drug loading (2% w/w), TBM was not detected in samples having the drug solubilized in the PEG phase (b-MPs@2H), whereas small TBM areas were detected in

formulations containing TBM loaded in the lipid phase (L-MPs and b-MPs@2L). The presence of TBM dispersed at the molecular level, in fact, is unlikely to determine intense Raman signals. The drug areas detected by CRM in a multicomponent pharmaceutical formulation depend on high concentration (intensity) of drug crystalline or amorphous particles [33,34]. Therefore, the presence of these small areas strongly suggested that TBM was dispersed as crystalline particles within the lipid phase of the MPs. This was not surprising as TBM, which was loaded as crystalline powder in the molten lipid producing a fine suspension, is likely to remain crystalline after spray congealing process.

Specifically, in L-MPs the distribution of TBM (red areas) within the lipid matrix (blue area) can be nicely observed. Thus, it can be concluded that in L-MPs TBM is (totally or mostly) crystalline and evenly distributed through the particle matrix.

Conversely, hybrid particles with drug loaded in the lipid phase (b-MPs@2L) were characterized by red areas on the external border of the PEG phases rather than in the PEG cores, as well as some red areas within the blue lipid region. Thus, in this system TBM is (at least partially) crystalline and distributed in the lipid phase or at the PEG/lipid interface.

Finally, in hybrid systems with drug solubilized in the PEG phase, the drug is preferentially localized in the PEG cores and (totally or partially) molecularly dispersed in the PEG phase. Specifically, when loaded at 2%, TBM is entirely molecularly dispersed in the PEG phase, as suggested by the absence of drug red spots in Raman mapping images as well as by the release behaviour (rapid and complete TBM release with supersaturation, Fig. 4 and Fig. 5b). Differently, at 4% and 10%, TBM is partially crystalline, as confirmed by the DSC results (Fig. 6), and partially solubilized in the PEG cores, as indicated by the CRM of b-MPs@4H and b-MPs@10*H*, showing the preferential distribution of the drug in the internal PEG phase.

Finally, Fig. 9 shows the drug release behavior of TBM from the MPs. When TBM was loaded into the lipid phase of the hybrid b-MPs (b-MPs@2L), the drug release was faster compared to pure lipid MPs with the same drug amount (L-MPs). This evidences the influence of the internal structure of the MPs in controlling the water diffusion through the particle matrix and therefore the drug release. Despite the different release behavior, no supersaturation was achieved when TBM was loaded as powder into the lipid phase (the TBM solubility limit is indicated by the blue line). Differently, the formulations having the drug solubilized in the PEG phase showed various release profiles depending on the drug loading amount. While for low drug loading (2%), rapid and complete drug release was observed with generation of supersaturated solution, for high drug loading b-MPs (10%), the drug released profiles was superimposed to the dissolution curve of the raw API. An intermediate behaviour was observed for b-MPs having 4% drug loading. The major influence of drug loading on the release behaviour of supersaturating formulations has been widely reported in the literature [35-38]. Specifically, a remarkable drop in drug release rate has been observed when a certain drug loading was reached. This abrupt change in release performance was found to be related with a switch from a polymer-controlled drug release kinetic (where drug and polymer dissolved simultaneously in the dissolution media), to a drug-controlled release kinetic whereby release of drug and polymer is incongruent [35,39]. Another plausible explanation to diminished dissolution performance of b-MPs with 4% and 10% drug loadings is the drug enrichment at the particle surface exposed to the dissolution medium. The generation of surface drug-enriched as a function of time has been observed for ASDs with high drug loadings [35,37,40] and might eventually lead to drug crystallization prior to dissolution, thus determining a decline in the dissolution rate.

Overall, the results highlight that the drug loading amount and location into b-MPs strongly impact the release performance of the dosage form.

4. Conclusion

Hybrid lipid-polymer MPs produced by an innovative *green* process based on spray congealing were investigated for the first time for the delivery of APIs having different hydrophilic/hydrophobic properties. In particular, we have investigated two hybrid MPs based on Compritol®888 ATO and cetylstearyl alcohol as external lipid phase and on PEG 400 as internal polymeric phase. The results evidenced that drug molecules affected the interactions at the lipid/PEG interface of the b-MPs without altering the cores-shell structure. Comparing to traditional one-phase lipid MPs, hybrid b-MPs showed a higher efficiency to encapsulate compounds with very different hydrophilic/hydrophobic properties, as well as a more differentiated array of release profiles depending on the type of drug, its location (inner or external phase), loading amount and particle composition. Among them, it is worth mentioning an enhanced release of tolbutamide, a BCS class II drug with moderate hydrophobicity, characterized by a rapid and complete release with concentration

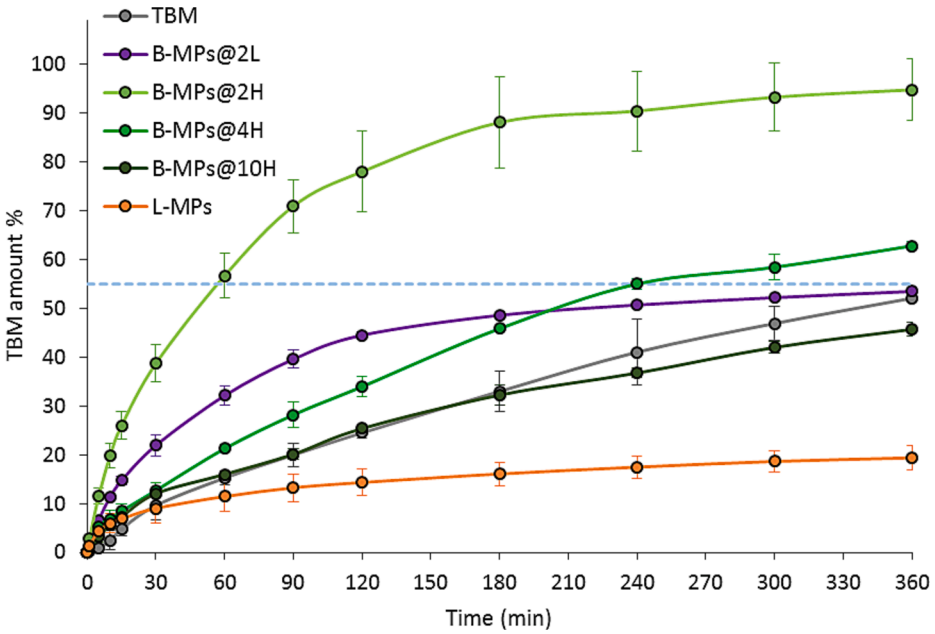

Fig. 9. Release profiles of tolbutamide from of hybrid particles with TBM loaded at various amount/locations (b-MPs@2H, b-MPs@4H, b-MPs@10*H* and b-MPs@2L) compared with one-phase lipid formulation containing 2% w/w of TBM (L-MPs), as well as release of pure drug (n = 3). All MPs samples had particle size 200–355 μm. The test is performed in non-sink conditions (SI = 0.7) and the dashed line represents the equilibrium solubility of crystalline TBM in the same dissolution medium.

exceeding drug solubility. Therefore, spray congealed lipid-based hybrid MPs are versatile systems able either to sustain the drug release, representing an alternative to other controlled-release multiparticulate dosage forms, or to enhance drug dissolution of poorly soluble drugs due to the formation of a supersaturated state, similarly to those obtained by self-emulsifying drug delivery systems or solid dispersions. Further steps will focus on the application of this formulation strategy for specific therapeutic needs, as for example oral combination therapies, where the simultaneous controlled release of two or more different drugs is required.

Overall, due to the highly customizable composition, facile and low-cost production, high encapsulation efficiency and tunable drug release, this study represents a proof of concept for the use of hybrid b-MPs produced by the spray congealing technology as a modified delivery platform for oral drug administration.

CRediT authorship contribution statement

Serena Bertoni: Conceptualization, Methodology, Investigation, Data curation, Formal analysis, Writing – original draft. **Beatrice Albertini:** Conceptualization, Methodology, Visualization, Supervision, Data curation, Writing – review & editing. **Joanna Ronowicz-Pilarczyk:** Methodology, Investigation, Data curation, Writing – review & editing. **Nadia Passerini:** Project administration, Funding acquisition, Supervision, Writing – review & editing.

Declaration of Competing Interest

The authors declare that they have no known competing financial interests or personal relationships that could have appeared to influence the work reported in this paper.

Data availability

Data will be made available on request.

Acknowledgements

Raman mapping was supported by the Nicolaus Copernicus University in Toruń under the Excellence Initiative - Debuts (grant IDUB 2020-1-NZ-Ronowicz).

Appendix A. Supplementary material

Supplementary data to this article can be found online at https://doi.org/10.1016/j.ejpb.2023.07.017.

References

[1] S. Scalia, P.M. Young, D. Traini, Solid lipid microparticles as an approach to drug delivery, Expert Opin. Drug Deliv. 12 (2015) 583–599, https://doi.org/10.1517/17425247.2015.980812.
[2] E. Mathiowitz, J.S. Jacob, Y.S. Jong, G.P. Carino, D.E. Chickering, P. Chaturvedi, C. A. Santos, K. Vijayaraghavan, S. Montgomery, M. Bassett, C. Morrell, Biologically erodable microspheres as potential oral drug delivery systems, Nature. 386 (1997) 410–414, https://doi.org/10.1038/386410a0.
[3] C. Vilos, L.A. Velasquez, Therapeutic strategies based on polymeric microparticles, J. Biomed. Biotechnol. 2012 (2012), 672760, https://doi.org/10.1155/2012/672760.
[4] O. Pillai, R. Panchagnula, Polymers in drug delivery, Curr. Opin. Chem. Biol. 5 (2001) 447–451, https://doi.org/10.1016/S1367-5931(00)00227-1.
[5] E. Lagreca, V. Onesto, C. Di Natale, S. La Manna, P.A. Netti, R. Vecchione, Recent advances in the formulation of PLGA microparticles for controlled drug delivery, Prog. Biomater. 9 (2020) 153–174, https://doi.org/10.1007/s40204-020-00139-y.
[6] J. Siepmann, A. Faham, S.-D. Clas, B.J. Boyd, V. Jannin, A. Bernkop-Schnürch, H. Zhao, S. Lecommandoux, J.C. Evans, C. Allen, O.M. Merkel, G. Costabile, M. R. Alexander, R.D. Wildman, C.J. Roberts, J.-C. Leroux, Lipids and polymers in pharmaceutical technology: lifelong companions, Int. J. Pharm. 558 (2019) 128–142, https://doi.org/10.1016/j.ijpharm.2018.12.080.
[7] D.M. Small, A classification of biologic lipids based upon their interaction in aqueous systems, J. Am. Oil Chem. Soc. 45 (1968) 108–119, https://doi.org/10.1007/BF02915334.
[8] B. Albertini, S. Bertoni, B. Perissutti, N. Passerini, An investigation into the release behavior of solid lipid microparticles in different simulated gastrointestinal fluids, Colloids Surf. B Biointerfaces. 173 (2019) 276–285, https://doi.org/10.1016/j.colsurfb.2018.09.056.
[9] B. Mandal, H. Bhattacharjee, N. Mittal, H. Sah, P. Balabathula, L.A. Thoma, G. C. Wood, Core–shell-type lipid–polymer hybrid nanoparticles as a drug delivery platform, Nanomed. Nanotechnol. Biol. Med. 9 (2013) 474–491, https://doi.org/10.1016/j.nano.2012.11.010.
[10] C. Wu, X. Luo, S.G. Baldursdottir, M. Yang, X. Sun, H. Mu, In vivo evaluation of solid lipid microparticles and hybrid polymer-lipid microparticles for sustained delivery of leuprolide, Eur. J. Pharm. Biopharm. 142 (2019) 315–321, https://doi.org/10.1016/j.ejpb.2019.07.010.
[11] S. Maghrebi, P. Joyce, M. Jambhrunkar, N. Thomas, C.A. Prestidge, Poly(lactic-co-glycolic) acid-lipid hybrid microparticles enhance the intracellular uptake and antibacterial activity of rifampicin, ACS Appl. Mater. Interfaces. 12 (2020) 8030–8039, https://doi.org/10.1021/acsami.9b22991.
[12] S. Han, P. Dwivedi, F.A. Mangrio, M. Dwivedi, R. Khatik, D.E. Cohn, T. Si, R.X. Xu, Sustained release paclitaxel-loaded core-shell-structured solid lipid microparticles for intraperitoneal chemotherapy of ovarian cancer, Artif. Cells Nanomed. Biotechnol. 47 (2019) 957–967, https://doi.org/10.1080/21691401.2019.1576705.
[13] P. Joyce, C.P. Whitby, C.A. Prestidge, Bioactive hybrid particles from poly(d, l-lactide-co-glycolide) nanoparticle stabilized lipid droplets, ACS Appl. Mater. Interfaces. 7 (2015) 17460–17470, https://doi.org/10.1021/acsami.5b05068.
[14] S. Maghrebi, M. Jambhrunkar, P. Joyce, C.A. Prestidge, Engineering PLGA–lipid hybrid microparticles for enhanced macrophage uptake, ACS Appl. Bio Mater. 3 (2020) 4159–4167, https://doi.org/10.1021/acsabm.0c00251.
[15] X.-T. Sun, R. Guo, D.-N. Wang, Y.-Y. Wei, C.-G. Yang, Z.-R. Xu, Microfluidic preparation of polymer-lipid Janus microparticles with staged drug release property, J. Colloid Interface Sci. 553 (2019) 631–638, https://doi.org/10.1016/j.jcis.2019.06.069.
[16] C. Karavasili, N. Bouropoulos, L. Sygellou, E.P. Amanatiadou, I.S. Vizirianakis, D. G. Fatouros, PLGA/DPPC/trimethylchitosan spray-dried microparticles for the nasal delivery of ropinirole hydrochloride: in vitro, ex vivo and cytocompatibility assessment, Mater. Sci. Eng. C. 59 (2016) 1053–1062, https://doi.org/10.1016/j.msec.2015.11.028.
[17] S. Bertoni, B. Albertini, J. Ronowicz-Pilarczyk, N. Calonghi, N. Passerini, Solvent-free fabrication of biphasic lipid-based microparticles with tunable structure, Pharmaceutics. 14 (2022), https://doi.org/10.3390/pharmaceutics14010054.
[18] N. Mehio, H.L. Frericks Schmidt, G.P.F. Wood, B.C. Hancock, R.M. Shanker, J. A. Bartlett, S.L. Shamblin, Binary isobaric phase diagrams of stearyl alcohol-poloxamer 407 formulations in the molten and solid state, Int. J. Pharm. 623 (2022), 121908, https://doi.org/10.1016/j.ijpharm.2022.121908.
[19] J. de A. Figueiredo, C.R. de P. Silva, M.F. Souza Oliveira, L.B. Norcino, P.H. Campelo, D.A. Botrel, S.V. Borges, Microencapsulation by spray chilling in the food industry: Opportunities, challenges, and innovations, Trends Food Sci. Technol. 120 (2022) 274–287. https://doi.org/10.1016/j.tifs.2021.12.026.
[20] E. Wolska, M. Brach, Distribution of drug substances in solid lipid microparticles (SLM)—methods of analysis and interpretation, Pharmaceutics 14 (2022), https://doi.org/10.3390/pharmaceutics14020335.
[21] H. Davies-Strickleton, J. Cook, S. Hannam, R. Bennett, A. Gibbs, D. Edwards, C. Ridden, J. Ridden, D. Cook, Assessment of the nail penetration of antifungal agents, with different physico-chemical properties, PLOS ONE. 15 (2020) e0229414.
[22] J.A. Baird, B. Van Eerdenbrugh, L.S. Taylor, A classification system to assess the crystallization tendency of organic molecules from undercooled melts, J. Pharm. Sci. 99 (2010) 3787–3806, https://doi.org/10.1002/jps.22197.
[23] K. Ullmann, L. Poggemann, H. Nirschl, G. Leneweit, Adsorption process for phospholipids of different chain lengths at a fluorocarbon/water interface studied by Du Noüy ring and spinning drop, Colloid Polym. Sci. 298 (2020) 407–417, https://doi.org/10.1007/s00396-020-04618-3.
[24] B. Albertini, N. Passerini, F. Pattarino, L. Rodriguez, New spray congealing atomizer for the microencapsulation of highly concentrated solid and liquid substances, Eur. J. Pharm. Biopharm. 69 (2008) 348–357, https://doi.org/10.1016/j.ejpb.2007.09.011.
[25] R.P. Gullapalli, C.L. Mazzitelli, Polyethylene glycols in oral and parenteral formulations—a critical review, Int. J. Pharm. 496 (2015) 219–239, https://doi.org/10.1016/j.ijpharm.2015.11.015.
[26] K. Bhesaniya, K. Nandha, S. Baluja, Thermodynamics of fluconazole solubility in various solvents at different temperatures, J. Chem. Eng. Data. 59 (2014) 649–652, https://doi.org/10.1021/je4010257.
[27] A. Schittny, J. Huwyler, M. Puchkov, Mechanisms of increased bioavailability through amorphous solid dispersions: a review, Drug Deliv. 27 (2020) 110–127, https://doi.org/10.1080/10717544.2019.1704940.
[28] A.-R. Ilie, B.T. Griffin, M. Vertzoni, M. Kuentz, R. Kolakovic, A. Prudic-Paus, A. Malash, H. Bohets, J. Herman, R. Holm, Exploring precipitation inhibitors to improve in vivo absorption of cinnarizine from supersaturated lipid-based drug delivery systems, Eur. J. Pharm. Sci. 159 (2021), 105691, https://doi.org/10.1016/j.ejps.2020.105691.
[29] D.D. Sun, H. Wen, L.S. Taylor, Non-sink dissolution conditions for predicting product quality and in vivo performance of supersaturating drug delivery systems, J. Pharm. Sci. 105 (2016) 2477–2488, https://doi.org/10.1016/j.xphs.2016.03.024.

[30] D.D. Sun, T.R. Ju, P.I. Lee, Enhanced kinetic solubility profiles of indomethacin amorphous solid dispersions in poly(2-hydroxyethyl methacrylate) hydrogels, Eur. J. Pharm. Biopharm. 81 (2012) 149–158, https://doi.org/10.1016/j.ejpb.2011.12.016.
[31] 5.17 Recommendations on Methods for Dosage Forms Testing, European Pharmacopoeia 8.0 (2010), in: n.d.: pp. 727–729.
[32] S. Baghel, H. Cathcart, N.J. O'Reilly, Understanding the generation and maintenance of supersaturation during the dissolution of amorphous solid dispersions using modulated DSC and 1H NMR, Int. J. Pharm. 536 (2018) 414–425, https://doi.org/10.1016/j.ijpharm.2017.11.056.
[33] H. Ueda, Y. Ida, K. Kadota, Y. Tozuka, Raman mapping for kinetic analysis of crystallization of amorphous drug based on distributional images, Int. J. Pharm. 462 (2014) 115–122, https://doi.org/10.1016/j.ijpharm.2013.12.025.
[34] C. Luebbert, C. Klanke, G. Sadowski, Investigating phase separation in amorphous solid dispersions via Raman mapping, Int. J. Pharm. 535 (2018) 245–252, https://doi.org/10.1016/j.ijpharm.2017.11.014.
[35] S. Saboo, N.A. Mugheirbi, D.Y. Zemlyanov, U.S. Kestur, L.S. Taylor, Congruent release of drug and polymer: a "sweet spot" in the dissolution of amorphous solid dispersions, J. Controlled Release. 298 (2019) 68–82, https://doi.org/10.1016/j.jconrel.2019.01.039.
[36] A.S. Indulkar, X. Lou, G.G.Z. Zhang, L.S. Taylor, Insights into the dissolution mechanism of ritonavir-copovidone amorphous solid dispersions: importance of congruent release for enhanced performance, Mol. Pharm. 16 (2019) 1327–1339, https://doi.org/10.1021/acs.molpharmaceut.8b01261.
[37] S. Saboo, D.E. Moseson, U.S. Kestur, L.S. Taylor, Patterns of drug release as a function of drug loading from amorphous solid dispersions: a comparison of five different polymers, Eur. J. Pharm. Sci. 155 (2020), 105514, https://doi.org/10.1016/j.ejps.2020.105514.
[38] S.V. Bhujbal, V. Pathak, D.Y. Zemlyanov, L.S. Taylor, Q. (Tony) Zhou, Physical Stability and Dissolution of Lumefantrine Amorphous Solid Dispersions Produced by Spray Anti-Solvent Precipitation, J. Pharm. Sci. 110 (2021) 2423–2431. https://doi.org/10.1016/j.xphs.2020.12.033.
[39] S. Saboo, U.S. Kestur, D.P. Flaherty, L.S. Taylor, Congruent release of drug and polymer from amorphous solid dispersions: insights into the role of drug-polymer hydrogen bonding, surface crystallization, and glass transition, Mol. Pharm. 17 (2020) 1261–1275, https://doi.org/10.1021/acs.molpharmaceut.9b01272.
[40] S. Saboo, P. Bapat, D.E. Moseson, U.S. Kestur, L.S. Taylor, Exploring the role of surfactants in enhancing drug release from amorphous solid dispersions at higher drug loadings, Pharmaceutics. 13 (2021), https://doi.org/10.3390/pharmaceutics13050735.